Design of a three-loop asymmetric coil producing a homogeneous radiofrequency B 1 field gradient along the axis of a vertical sample tube

Laouès Guendouz, Sebastien Leclerc, Pierre-Louis Marande, Alain Retournard, Daniel Canet

Design of a three-loop asymmetric coil producing a homogeneous radiofrequency B_1 field gradient along the axis of a vertical sample tube

Laouès Guendouz[1,2*], Sébastien Leclerc[1,2], Pierre-Louis Marande[3,4], Alain Retournard[3,4], Daniel Canet[1,2]

[1] Université de Lorraine, LEMTA, UMR 7563, Vandœuvre-lès-Nancy, F-54500, France
[2] CNRS, LEMTA, UMR 7563, Vandœuvre-lès-Nancy, F-54500, France
[3] Université de Lorraine, CRM2, UMR 7036, Vandœuvre-lès-Nancy, F-54506, France
[4] CNRS, CRM2, UMR 7036, Vandœuvre-lès-Nancy, F-54506, France

E-mail : laoues.guendouz@univ-lorraine.fr

Abstract
A coil system generating a vertical radio-frequency (rf) field gradient (B_1 gradient) has been built for surrounding, in a horizontal magnet, a vertical sample (object) of axial symmetry. The system comprises three coaxial loops with an overall shape either spherical or ellipsoidal. The geometry has been theoretically and experimentally devised for producing a very uniform gradient (cancellation of B_1 derivatives from second order up to sixth order) in the central region where a vertical receiver/transmitter coil is installed. The latter is of the saddle-shaped type and is geometrically and electrically decoupled from the gradient coil system. This receiver/transmitter coil not only ensures an optimal signal reception but, in addition, is able to deliver perfectly homogeneous rf hard pulses which are mandatory in most NMR experiments. In its present design, the system delivers a uniform gradient in a limited region but could be extended at will. Its main advantages over static field gradients (B_0 gradients) appear clearly in the case of very short transverse relaxation times. This property has been emphasized in the case of experiments leading to the measurement of diffusion coefficients. Also, this system would be suitable for chemical shift imaging (CSI) experiments as confirmed by a preliminary test experiment.

Keywords
radio-frequency field gradient, dedicated radio-frequency coils, diffusion measurements, 1D profiles

INTRODUCTION

The use of magnetic field gradients in NMR is ubiquitous. It is mandatory in MRI. Most of the time, gradients of the static magnetic field (also called B_0 gradients) are employed essentially because they can be applied indifferently in the three spatial directions and because, thanks to a highly developed technology, they can be easily manipulated. Although possessing some distinct advantages (to be discussed below) [1], the gradients of the radio-frequency magnetic field (also called B_1 gradients) have enjoyed far less success. It can be thought that the main reason for this disaffection lies in the difficulty to apply these gradients in the three spatial directions due, *inter alia*, to the fact that the B_1 field is necessarily perpendicular to the B_0 direction. Nevertheless, B_1 gradients possess some unique properties which are in contrast with B_0 gradients: i) their rise and fall times are negligibly small, ii) they are immune to magnetic susceptibility effects, iii) they can act on any component of the nuclear magnetization. This has constituted the incentive to develop B_1 gradient systems devised for spatial localization and subsequent specific applications. Often, these have been single-sided flat coil(s) used to produce a B_1 gradient which is possibly perpendicular to the sample [2-10]. However, with these arrangements, the gradient may not be uniform in a sufficiently large region (with respect to the object to be investigated). Furthermore, the uniformity of the B_1 field within planes perpendicular to the gradient direction is far from being warranted. Relatively recently [11], a tapered strapline device has been shown to deliver a very uniform (and possibly intense) B_1 gradient still in a single-sided way. This device, quite appealing, is however used as transmitter and receiver which implies receptivity corrections and precludes its use for generating classical hard pulses generally employed in NMR or MRI along with gradient methodology. By contrast, some time ago [12], we proposed a single-sided two-coil system able to deliver a very uniform B_1 gradient, as well as a uniform B_1 field in planes perpendicular to the gradient direction. This experimental

configuration involves also a conventional saddle-shaped coil for usual transmit-receive NMR/MRI operations. Other devices for producing B_1 gradients include straddle coil (*i.e.* anti-Helmoltz coils) with the inconvenience of zero rf field at the center of the coil assembly [13,14] and a toroid cavity by which strong but non-uniform gradients are obtained [15]. Also, conic coils have been widely employed although they generally deliver an approximately uniform B_1 gradient with strong variations of the rf field in planes perpendicular to the main gradient direction. This type of coil can be positioned around the sample [16-20] or remotely along the sample axis [21,22].

The aim of the present work is the construction of a high-performance B_1 gradient system, able to surround a cylindrical sample/object so that the latter could be investigated along the symmetry axis direction. The probe design is along the same lines as the single-sided probe previously constructed [12] but, this time, it involves three loops (instead of two) still with a standard receive/transmit coil in the center of the assembly. The latter is geometrically and electrically decoupled from the three-loop gradient system and, in addition to acquire reliably the NMR signal, serves for any pulse sequence requiring homogeneous hard pulses. The three-loop gradient system has been carefully calculated and designed for delivering a very uniform B_1 gradient together with a very uniform B_1 field in planes perpendicular to the gradient direction. This device can be used in horizontal and vertical magnets, the B_1 gradient being in each instance perpendicular to the static magnetic field B_0. The advantages of the three-coil system in comparison with the two-coil system will be presented here. For convenience, because we shall be dealing with samples containing fluids, tests were performed with a horizontal magnet. These tests will include the measurement of diffusion coefficients and a prospective experiment aiming at Chemical Shift Imaging. Although it could presumably be enlarged, the zone where the gradient is uniform is presently of the order of some centimeters which is nevertheless sufficient for standard NMR tubes.

B_1 GRADIENT DESIGN AND CALCULATIONS

First, it can be recalled that, in the case of a simple circular loop (denoted SL) of radius a located at an abscissa $a/2$ with respect to the origin O (see Fig. 1), the magnetic field along the *x*-axis perpendicular to the loop and positioned at its center can be easily calculated from the Biot-Savart law and approximated as follows (with rounded coefficients)

$$B_{1,axial}^{SL} \approx \left(\frac{\mu_0 I}{a}\right)\left[0.358 + 0.429\left(\frac{x}{a}\right) - 0.458\left(\frac{x}{a}\right)^3 - 0.412\left(\frac{x}{a}\right)^4 + \cdots\right] \quad (1)$$

where I is the current intensity in the loop and μ_0 the air permeability.

From the derivative (with respect to x) of (1), we obtain the expression of the B_1 gradient, only homogeneous up to the second order.

$$G_1^{SL} \approx \left(\frac{\mu_0 I}{a^2}\right) 0.429\left[1 - 3.20\left(\frac{x}{a}\right)^2 - 3.84\left(\frac{x}{a}\right)^3 + \cdots\right] \quad (2)$$

From Eq. (2), it appears that the gradient is uniform (to within 1%) in a relatively small interval: $[-0.058a, 0.054a]$. Although the single loop configuration is easy to implement, its modest performance in terms of useful volume and efficiency (G_1^{SL}/I at the origin O) is noteworthy.

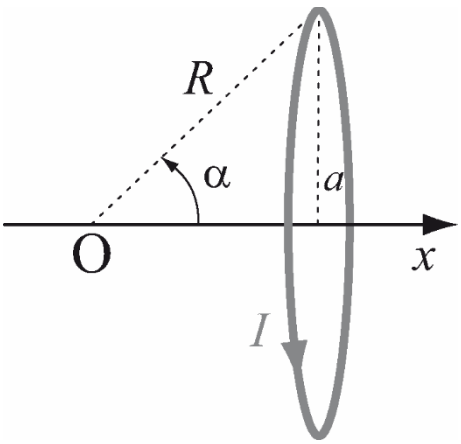

Fig. 1. Geometry of a general current loop carrying a current I, with radius a and symmetry axis O*x* (at a radial distance R from the origin and subtending an angle α with *x*-axis).

Although the gradient characteristics can be improved by a single-sided two-coil system [12], it seems advisable to go to a three-loop system not only to improve the gradient but also to give up with the single-sided feature in such a way that the coil assembly can surround the object under investigation (Fig. 2).

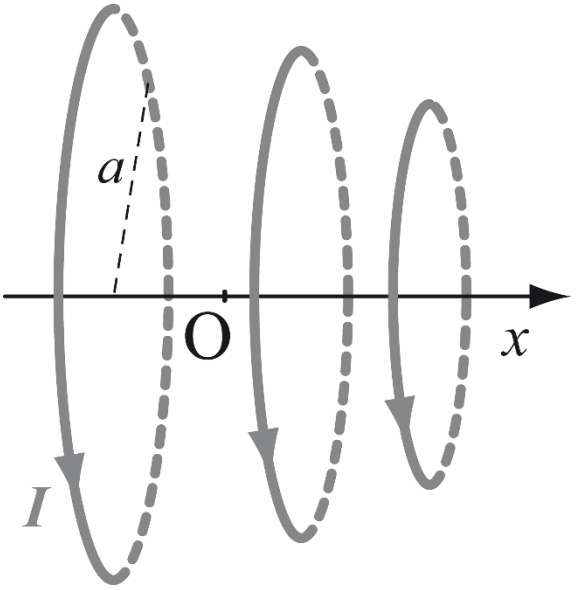

Fig. 2. A simple sketch of a three-loop system

Evidently, this may require further investigations and somewhat lengthy calculations which are detailed in the Appendix. From these calculations, we can derive the expression of the B_1 field for a configuration such that three loops are positioned within a sphere (configuration denoted TL_S) and for an optimized configuration where an ellipsoid replaces the sphere (denoted TL_E):

$$B_{1,axial}^{TL_S} \approx \left(\frac{\mu_0 I}{a}\right)\left[1.0875 + 0.9739\left(\frac{x}{a}\right) - 1.1226\left(\frac{x}{a}\right)^5 - 1.1610\left(\frac{x}{a}\right)^6 + \cdots\right], \qquad (3)$$

$$B_{1,axial}^{TL_E} \approx \left(\frac{\mu_0 I}{a}\right)\left[1.2189 + 0.9836\left(\frac{x}{a}\right) - 3.1954\left(\frac{x}{a}\right)^7 - 7.6444\left(\frac{x}{a}\right)^8 + \cdots\right] \qquad (4)$$

where a is the radius of the largest coil.

We turn now to the gradient of B_{1x} along the x direction, having in mind that its quality rests on two main features: its strength and its uniformity. Concerning configuration TL_S, the

gradient is homogeneous up to fourth order and can be expressed as follows (with rounded coefficients)

$$G_{1,axial}^{TL_S} \approx \left(\frac{\mu_0 I}{a^2}\right) 0.9739[1 - 5.764\left(\frac{x}{a}\right)^4 - 7.153(\frac{x}{a})^5 + \cdots]. \quad (5)$$

On the other hand, for the configuration TL_E , the gradient is homogeneous up to sixth order and can be written:

$$G_{1,axial}^{TL_E} \approx \left(\frac{\mu_0 I}{a^2}\right) 0.9836[1 - 22.74\left(\frac{x}{a}\right)^6 - 62.17(\frac{x}{a})^7 + \cdots]. \quad (6)$$

In any case, using closed-form expression, it appears that the gradient is uniform (in the limit of 1%) in a relatively large interval $[-0.223\ a, 0.195\ a]$ for configuration TL_S, and in a larger interval for configuration TL_E: $[-0.333\ a, 0.253\ a]$.

Now, if a deviation of 10% can be envisioned, we have the following intervals: for SL $[-0.203\ a, 0.163\ a]$, for TL_S $[-0.452\ a, 0.342\ a]$ and for TL_E $[-0.577\ a, 0.367\ a]$.

On the whole, although all these uniformity intervals are not rigorously centered on the origin O, the three coil systems are seen to be noticeably advantageous. In this respect, the gradient uniformity (along the symmetry axis) is visualized in Fig. 3 for the probes considered in this work.

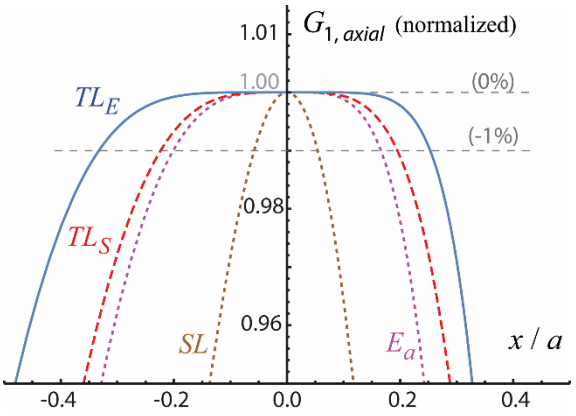

Fig. 3. Computed normalized rf field gradient $G_{1,axial}$: profiles along the symmetry axis for the three-coil systems TL_E (solid line in blue) and TL_S (dashed line in red), for an optimized two-loop system [12] E_a (dotted line in purple) and for a single loop SL (dotted line in brown). For the four systems, a is the radius of the outer coil.

It must be noted that these calculations performed for a direct current remain valid in the radio-frequency domain provided that the overall dimension of the coil system and of all elements constituting this device remain small with respect to the wavelength associated with the working frequency. This is further discussed in forthcoming section "Prototype".

PROPERTIES OF THE MAGNETIC FIELD AND OF ITS ASSOCIATED GRADIENT FOR THE THREE-COIL ARRANGEMENTS TL_S AND TL_E

In the following, to facilitate comparisons, we shall consider devices which occupy the same space with respect to the axial symmetry axis. In practice, this amounts to take as reference the outer loop of radius denoted by a as before. The dimensions of the different loop configurations studied in this work are reported in Table A2 of the Appendix.

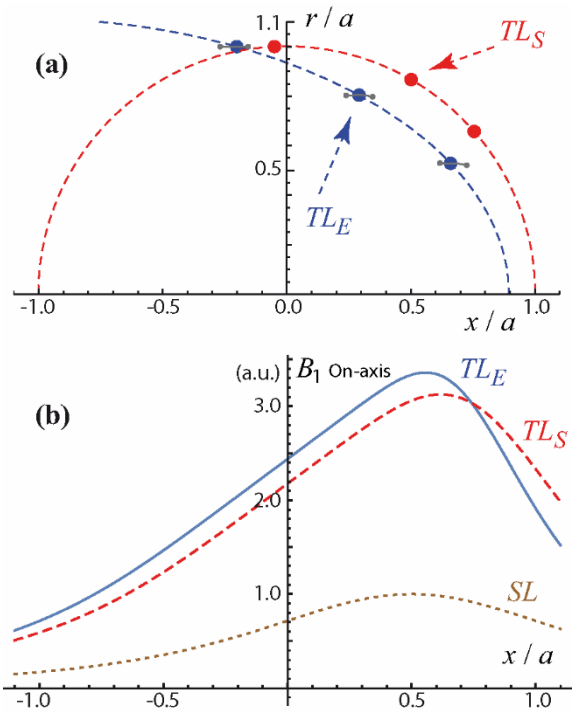

Fig. 4. (a) Cross-sectional view, through an axial symmetry plane, of the coil systems TL_S (upper curve, in red) and TL_E (lower curve, in blue). Loop positions are marked by bold dots and dashed lines indicate the surface surrounded the coils (spherical or ellipsoidal). (b) Curves of the on-axis magnetic field for the coil systems TL_E (solid line in blue), TL_S (dashed line in red) and a single loop SL as defined in the text (dotted line in brown), for comparison. All the coils have the same outer radius a and are driven by the same current I.

Fig. 4(a) depicts the geometry of the two configurations TL_S and TL_E for the same value of radius a (radius of the outer loop). The B_1 magnetic field profile along the Ox axis is shown in Fig. 4(b) for these two configurations with, for the sake of comparison, the B_1 profile corresponding to a single loop SL. These profiles have been calculated by assuming an identical current I in these coil systems. First, it can be noticed that the ellipsoidal three-coil configuration affords, at the origin O, a B_1 field larger by a factor of 3.4 than the one produced by a single coil. Moreover, the B_1 gradient (G_1) is seen to be more uniform and anyway greater by a factor of 2.3.

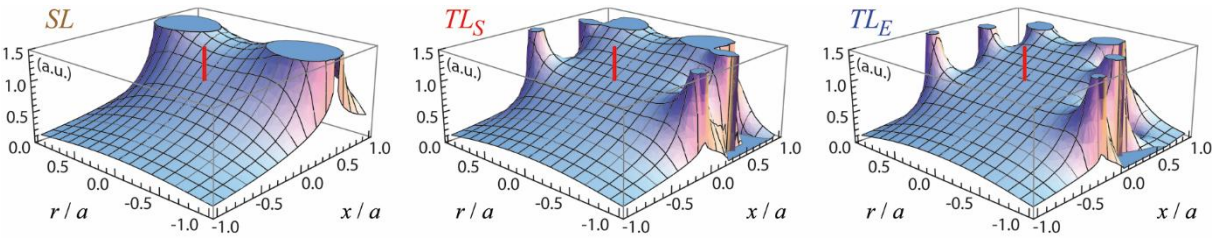

Fig. 5. 3D representation, corresponding to a *rx*-plane (any plane containing the symmetry axis x**)**, of the axial component B_{1x} of the magnetic field produced by the coil systems (see text): configurations TL_S, TL_E and SL. Position of the origin O is marked by a centered vertical line (in red). For all configurations, the outer coil has the same radius a. The three coil systems are assumed to be driven by the same current I.

The axial component B_{1x} of the rf magnetic field [23], in a plane containing the x symmetry axis, is displayed by means of a 3D plot in Fig. 5 for the three usual configurations SL, TL_S and TL_E (same radius a and same current I). These plots allow one to appreciate the uniformity of B_{1x} in planes perpendicular to the gradient direction (the x direction). Configuration TL_E appears undoubtedly to be optimal.

From the analytical expression of the components of the magnetic field produced by a coil [23], it is possible to calculate the axial component of the field gradient at any point. Contour plots showing the deviation of the value of this component with respect to its value at the origin are displayed in Fig. 6 for our usual three systems. It can be observed that, in the Ox

direction, the gradient tends to decrease when the distance to the origin increases whereas it is the opposite behavior in a direction perpendicular to O*x*.

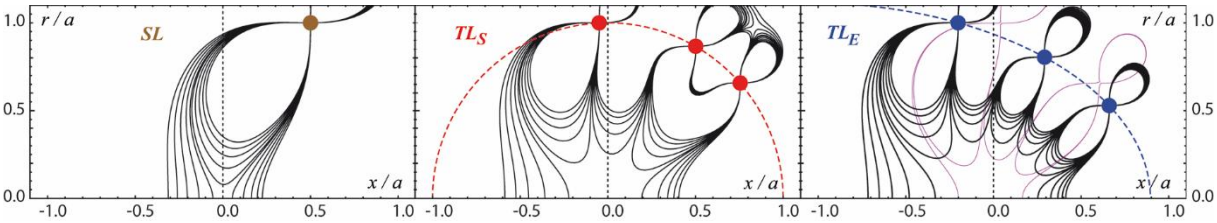

Fig. 6. Contour plots of the deviation of the axial gradient G_{1x} from the value at center represented in an arbitrary axial symmetry plane (containing the gradient direction). Successive iso-gradient contours correspond to deviations of ±1% (close to center), ±5%, ±10%, ±15%, ±20% (far from center). These contour plots are displayed for the usual configurations: SL, TL_S and TL_E.. The geometry of each configuration is schematized by color dots indicating the location of the loops (see fig. 4a). Both axes have the same scale (relative to the radius a of the main loop). In the last case, the thin inner curve (purple) corresponding to the ±1% contour plot for the optimal two-coil E_a (with outer diameter a) [12] is added for comparison.

As shown previously [12], the other two components of the B_1 field (namely B_{1y} and B_{1z}) can be neglected in the region surrounded by the additional coil used for the NMR signal detection (and for delivering homogeneous rf pulses). As a matter of fact, these non-axial components become significant far outside the region occupied by the three-coil system. Thus, from an NMR point of view, the above discussion is perfectly valid.

At this point, a more in-depth comparison between the optimum two-loop system (dubbed E_a in figures 6 and 7) described in our previous paper [12] and the present TL_E system is necessary. On a quantitative point of view, figure 7(a) shows the geometries of the two gradient coils with same outer diameter, and figure 7(b) the corresponding on-axis magnetic field which is in favor of the TL_E system. Moreover, the gradient field uniformity area as well as the gradient value are displayed in figure 7(c), and demonstrate definitely the superiority of the TL_E system.

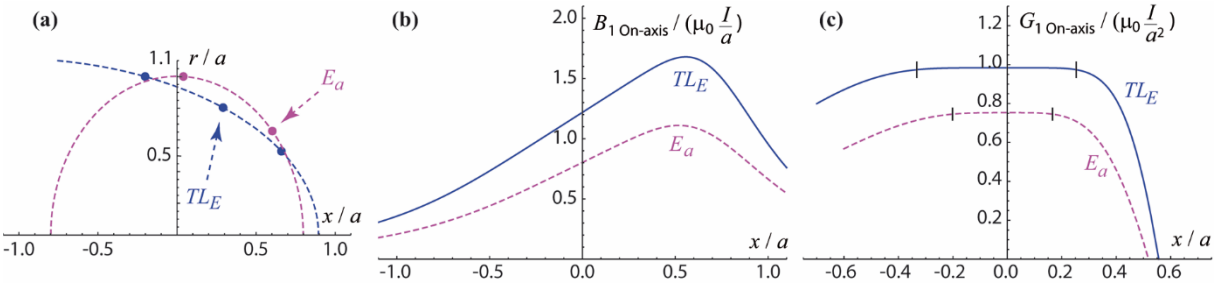

Fig. 7. (a) Cross-sectional view, through an axial symmetry plane, of the coil systems E_a (upper curve, in purple) [12] and TL_E (lower curve, in blue). Loop positions are marked by bold dots and dashed lines indicate the surface surrounded the coils (ellipsoidal). (b) Curves of the on-axis magnetic field (normalized to $\mu_0 I/a$) for the coil systems TL_E (solid line in blue), E_a (dashed line in magenta). The coils have the same outer radius a and are driven by the current I. (c) Computed field gradient $G_{1,axial}$ (normalized to $\mu_0 I/a^2$): profiles along the symmetry axis for the coil systems TL_E (solid line in blue) and E_a (dashed line in purple). The vertical bars delimit the 1% uniformity interval.

Moreover, given the common variation in (I/a^2) of the gradient field intensities (see Eq. (6)) comparisons can be made between the two coil systems when carrying the same current I.The optimum three-loop coil presents significant advantages: i) a 30 percent higher gradient field intensity ii) a 60 percent wider on-axis interval of gradient field uniformity at 1% iii) a gradient field uniformity area more centered to the coil system.

Now, for the same area of gradient field uniformity at 1% along the principal axis, the TL_E coil should be 37.5% smaller and would produce an approximately 234% higher gradient field intensity.

RF PROTOTYPE

For diffusion measurements and with the prospect of Chemical Shift Imaging on standard NMR samples, a prototype of the TL_E rf gradient system has been designed to operate in a Bruker Biospec mini-imager equipped with a 2.34 T horizontal magnet featuring a cylindrical working space of 20 cm diameter. The proton resonance frequency being of 100.3 MHz, the corresponding wavelength λ is about 3 m. A good compromise between the available dimensions of the working space and a realistic construction of our gradient system has been

found for an outer coil of diameter $2\,a = 5cm$ (see Table A2 of the Appendix for the dimensions of the other two coils). These dimensions afford a uniform gradient (in the 5% limit) over a length of about 2 cm. For transposing the results of the previous sections (strictly valid for direct current) to the radio-frequency case, the wires constituting the coil system must have a length less than $\lambda/10$ (if possible, less than $\lambda/20$). According to this constraint, we have chosen a single series resonant circuit (same current in all wires) with two identical tuning capacitors Ct_1 and Ct_2 separating symmetrically the outer loop from the other two loops (see Fig. 8a).

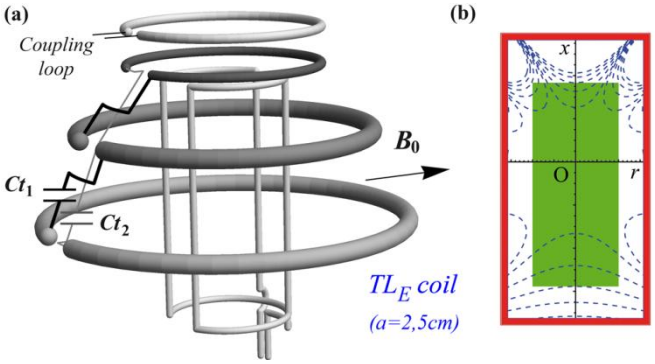

Fig. 8. (a) Schematic diagram of the rf gradient coil prototype (type TL_E) with balanced tuning capacitors Ct_1 and Ct_2, and a tuned matching coupling loop. A saddle-shaped coil (diameter: 1.65cm, height: 3.3cm) is used for normal transmit-receive NMR operations. (b) Overview of the deviation of the gradient field in an axial section of the saddle-shaped coil: iso-gradient contours are extracted from Fig. 6. The deviation from the maximum gradient value is less than 10% in a cylindrical volume with 1 cm in diameter and 2.4 cm in height (represented by a green filled rectangle).

This probe has been designed for accommodating objects (*e.g.* NMR tubes) positioned vertically. In order to obtain a good quality factor, the wire of the smallest coil has a diameter of 2 mm while a diameter of 4 mm has been retained for the other two coils. Matching is achieved by a coupling loop identical to the smallest loop of the gradient system, located axially and on the same side as the latter. This additional coil is tuned to the working frequency by a series capacitor. In that way, the gradient system is electrically balanced [24], as shown by the electrical scheme of Fig. 9.

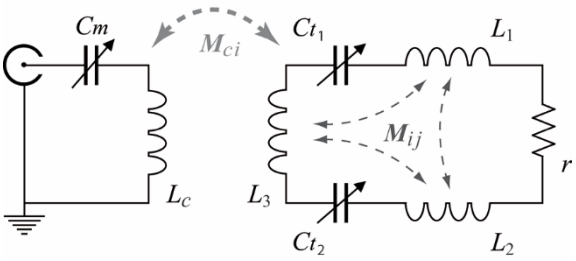

Fig. 9. Equivalent circuit model of the gradient three-coil system with its self-inductances L_i ($i = 1,2,3$), the mutual inductances M_{ij} ($i \neq j = 1,2,3$) and its symmetric tuning capacitors Ct_1 and Ct_2. The resistor r accounts for losses in the gradient coil system. Matching is achieved by a moveable tuned coupling loop. Both primary and secondary circuits are tuned to the Larmor frequency. Magnetic couplings are indicated by dashed lines.

Normal transmit-receive NMR operations are made possible by a saddle-shaped coil of 1.65 cm diameter and 3.3 cm height. It is made with a wire of 1.5 mm diameter. This coil is positioned vertically as a function of the gradient uniformity. As can be seen from Fig. 8(b), the gradient is quasi-uniform (in the limit of 1%) in a large central region and the uniformity remains in a limit of 5% in a region of 1 cm diameter and 2cm height. For obtaining the best gradient uniformity in the sensitive region of the saddle-shaped coil, the center of the latter has been shifted by 2 mm with respect to the origin O of the gradient system. Owing to these considerations, the diameter of the sample tube must not exceed 14 mm. Finally, the transmit-receive coil is classically tuned and matched by capacitors including a leg capacitor ensuring the electrical symmetry and thus a very good decoupling from the coils of the gradient system.

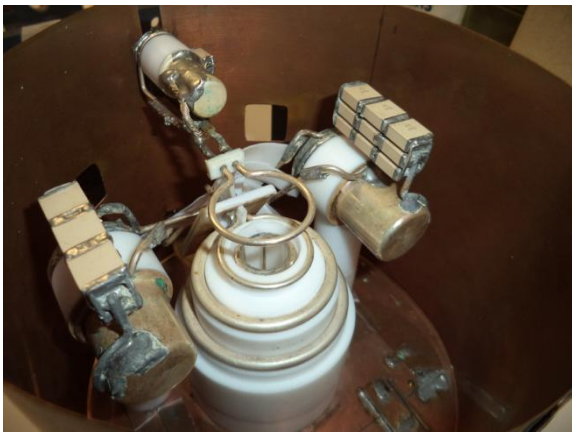

Fig. 10. Photograph of the rf gradient coil prototype operating in a horizontal magnet at 100.3 MHz. The upper part of the cylindrical shield was removed for observation. On either side of the three-loop coil (type TL_E with a diameter $2\ a = 5\ cm$) are mounted the tuning capacitors: a fixed ceramic capacitors assembly in parallel with a high voltage cylindrical tunable capacitor. A moveable tuned coupling loop is placed above the gradient coil for matching and a transmit-receive saddle shape coil is visible on the inside.

A photograph of the prototype is shown in Fig. 10. It is surrounded by a cylindrical copper shield (height: 11.5 cm, diameter: 14 cm), the top of which being removable for performing different operations such as decoupling (or taking photographs). This probe has been constructed with several guiding Teflon and glass pieces to facilitate its disassembly.

As an indication, according to the legend of figure 9, the inductance of the three-loop coil is given by:

$$L = L_1 + L_2 + L_3 + 2(M_{12} + M_{13} + M_{23}) \quad (7)$$

By using standard formulas for (rf) inductances and mutuals [24], the total inductance reduces to:

$$L \approx \mu_0(2.692\ a + a_1 \mathrm{Log}[a_1/\rho_1] + a_2 \mathrm{Log}[a_2/\rho_2] + a\ \mathrm{Log}[a/\rho_3]) \quad (8)$$

where ρ_i is the wire radius of loop i ($i = 1,2,3$). Thus, without taking into account junction wires, possible couplings and stray capacitances, we find 265 nH for the theoretical inductance of our three-loop system and predict an approximate value for the tuning capacitors Ct_1 and Ct_2, corresponding to $Ct_{1,2} \approx 19.1pF$.

More generally, when considering a ratio a/ρ_i of about $1/10$, the inductance can be written simply $7.55\ \mu_0 a$ which is about 67% higher of the value for the two-loop system E_a (see Eq. (15) in ref. [12]). Note that, for ratios a_i/ρ_i ($i = 1,2,3$) of about $1/10$, the increase is almost the same. This leads for the TL_E system to weaker tuning capacitors, and possibly a higher Q factor or a longer response time (coil ringing). Taking into account the discussion in the previous section, if necessary, it is possible to reduce the inductance of the TL_E system by reducing the size of the loops while maintaining good performance in terms of gradient field

uniformity and intensity, when compared to the two-loop system E_a. Thus, a good compromise between electrical performance and gradient field quality can be found.

Finally, in practice, the probe being inside the shield, tuning could be achieved with test capacitors of about 15pF. As shown in Fig. 10, the tuning capacitors are an assembly of fixed non-magnetic ceramic capacitors of 6.8pF (100E series, American Technical Ceramics, Huntingdon Station, NY ; Peak working volts 3.6kV) and of a 5-25pF variable capacitor (RP series, Polyflon, Norwalk, CT ; Peak working volts 10kV). In this way, the system can cope with high over-voltage arising from high input power (typically 300W-1kW). The role of fixed capacitors is to reduce the current in the variable capacitors. Concerning the coupling coil, tuning is carried out with a 0.5-10 pF variable capacitor (RP series, Polyflon). The quality factor, measured in unloaded conditions by means of a network analyzer at a frequency of 100.3 MHz, is of 512 for the three-loop system and 254 for the saddled-shape coil.

In theory, the magnetic coupling between these two "orthogonal" coil systems is zero, however, in practice, due to small misalignments and connection wires a weak coupling is observed. Rather than the mutual inductance which is not a significant feature, the isolation factor between the gradient system and the transmit-receive coil has been measured with a vectorial network analyzer, it remains greater than 35 dB. Thus, for a given RF power on one of the coils, the other one will receive less than three thousandth of this RF power. This good decoupling was obtained by a fine geometric adjustment of the two RF coil systems.

For checking the rf field (and its gradient) produced by the three-loop system, we have measured in free space the voltage induced in a pick-up coil that we displaced along the symmetry axis of the system. In a compromise between detection and decoupling, the pick-up coil consisted of a 5 mm circular loop of enameled copper wire with diameter 0.8 mm, the wires at the ends of the loop were twisted over 10 cm. A network analyzer, in the transmission

mode, was inserted between the gradient coil and the pick-up coil. Thus, the measured quantity represents essentially the mean magnetic field across the section of an axial cylinder with diameter corresponding to one-tenth the outer diameter of the gradient coil. The result, shown in Fig. 11, is seen to be consistent with the theoretical on-axis curve of the magnetic field.

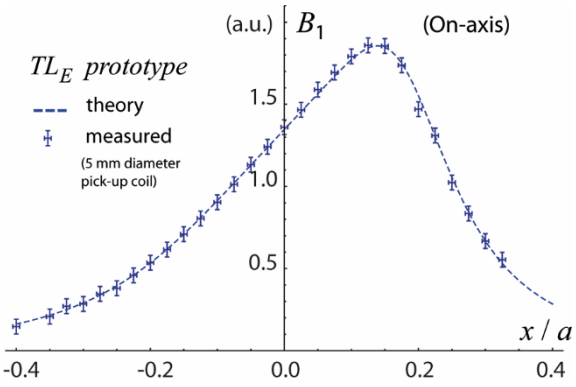

Fig. 11. Measured profile of the on-axis magnetic field produced by the TL_E three-coil prototype. Measurements were carried out in free space using the pick-up coil described in the text. Dashed line represents the normalized theoretical curve (see Fig. 4b).

Of course, this measurement does not take into account the actual environment of the probe, namely, its shield, the bore magnet or even the sample itself. In any case, NMR diffusion measurements (of large samples) should confirm the quality of the gradient field.

Note that, for our prototype, we have considered rather large dimensions. However, for increasing the gradient field intensity, it would be possible to reduce the dimensions by a factor of 2 or even 3 and obtain, for the same carrying current I, a gradient intensity 4 to 9 times greater and moreover be free from segmentation problems and alternatively achieve matching and tuning by direct capacitive coupling.

NMR EXPERIMENTS

Here, our objective is simply to go beyond methodological tests for assessing the properties of our new device through "real" classical NMR measurements. Possibly, we shall emphasize the ease of the B_1 gradient method.

Diffusion measurements

A first test is to perform a translational diffusion measurement according to the B_1 gradient methodology [1]. This simple experiment consists of applying two gradient pulses of duration δ separated by a diffusion interval Δ (from the end of the first gradient pulse till the beginning of the second gradient pulse), followed by a classical 90° observing pulse and data acquisition. The signal amplitude is given by

$$S(\delta,\Delta) \propto \exp\left(-\frac{\Delta}{T_1}\right)\exp(-\frac{2\delta}{T_{2\rho}})\exp[-\gamma^2 G_1^2\, D(\Delta+2\delta/3)] \qquad (9)$$

where T_1 is the classical longitudinal relaxation time, $\frac{1}{T_{2\rho}} = (\frac{1}{2})(\frac{1}{T_1}+\frac{1}{T_2})$ is the transverse relaxation time in the rotating frame (T_2 being the classical transverse relaxation time), γ the gyromagnetic ratio and G_1 the gradient strength. An example of such a measurement, obtained by varying δ, is given in Fig. 12. The perfect decay of the diffusion curve is a clear indication of the gradient quality.

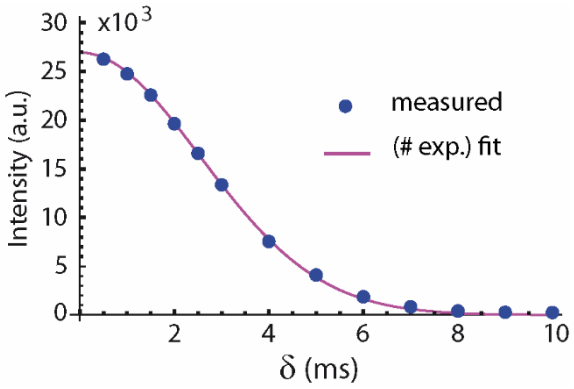

Fig. 12. A typical diffusion experiment performed on a water sample with the B_1 gradient system described above. The horizontal scale corresponds to the δ values in ms. Δ is set to 0.4 s. The dead time of the three-coil system is about 6.5 µs , and the RF amplifier power used for the experiments was about 150 W. With a diffusion coefficient of 2 10^{-5} cm^2s^{-1}, we obtain a

gradient value of 3.8 G cm^{-1}. Owing to the large difference between δ and Δ values, $\exp(-\frac{2\delta}{T_{2\rho}})$ was considered as constant and $(\Delta + 2\delta/3)$ was assimilated to Δ.

It can be remembered that diffusion measurements by B_1 gradients are formally equivalent to the widely used stimulated spin echo sequence by B_0 gradients. But this is just a formal equivalence. While the B_1 gradient method involves two gradient pulses separated by the diffusion interval Δ followed by a $\pi/2$ observing pulse, with the B_0 method, each gradient pulse must be bracketed by two $\pi/2$ pulses. Moreover, for avoiding the effect of internal gradients, the B_0 gradient pulse is generally replaced by the so-called bipolar pulses (two gradient pulses of opposite sign separated by a π hard pulse). This does not occur with B_1 gradients which are totally immune to variations of magnetic susceptibility within the sample (responsible for internal B_0 gradients). At the outcome, the B_0 gradient method generally ends up with a time interval called "led" for avoiding effects of eddy currents generated by the fall of the B_0 gradient. This is not evidently the case for B_1 gradients whose rise and fall times are negligibly short. As a matter of fact, a failure of B_0 gradients may occur in particular situations while B_1 gradients still fit the bill [25]. The advantages of the B_1 gradient methodology have been well documented until now with however a gradient perpendicular to the sample tube. It was worth, within the present context, to verify that these properties still hold with a gradient along the vertical axis of the sample tube. Furthermore, for assessing the properties of B_1 gradients, diffusion measurements by incrementation of the gradient were carried out in the case of a sample for which B_0 gradients totally failed (at least with gradients available with our spectrometer: $\leq$ 20 G/cm). In the case of very short T_2's (see below), the NMR signal disappears because it is destroyed by transverse relaxation during the fall time of the B_0 gradient pulses. We were dealing with a water sample containing 4mM of $MnCl_2$ providing a T_1 value of 50ms and a T_2 value of 3ms. This short value of T_2 explains the failure of B_0 gradient experiments for which the NMR signal is so deteriorated that any

diffusion measurement turns out to be impossible. By contrast, since the rise and fall times of B_1 gradient pulses are totally negligible, diffusion measurements become feasible by this method. The experiment was performed with gradient pulses of duration δ =2 ms and a diffusion interval Δ= 50 ms. Nine gradient values ranging from 0.5 G/cm up to 3.3 G/cm were used for obtaining a diffusion curve compatible which the usual value of the water diffusion coefficient.

One-dimensional Chemical Shift Imaging (CSI)

Another way for assessing the gradient quality is the sequence of figure 13, which is very simple and leads to the result given in figure 14.

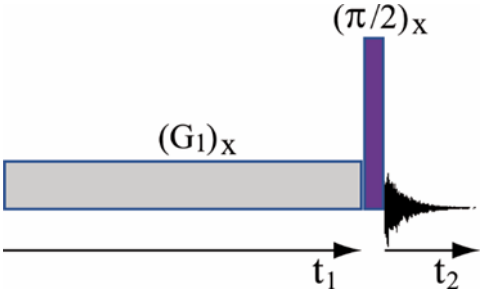

Fig. 13. Basic sequence for a two-dimensional experiment involving a B_1 gradient (G_1). Phases of the B_1 gradient pulse and of the $\pi/2$ pulse (optional) must be identical. t_1 is incremented so as to form a 2D map (t_1 , t_2) which is further subjected to a double Fourier transform. This pulse leads to a cosine modulation in the spatial dimension (perhaps more convenient for data treatment). Without it, one would have a sine modulation.

The sequence of figure 13 involves as many experiments (with incrementation of the time interval t_1) as necessary for the required spatial resolution. The signal obtained by this sequence has the form (quadrature detection assumed, ν_0 : resonance frequency in the chemical shift dimension; $f(\nu_0)$: free induction decay (fid) of the corresponding NMR signal):

$$S(t_1, t_2) = \int \rho(Z) \cos(\gamma G_1 Z t_1) e^{-t_1/T_{2\rho}} dZ \int f(\nu_0) \exp(2i\pi\nu_0 t_2) e^{-t_2/T_2^*} d\nu_0. \qquad (10)$$

The double Fourier transform with respect to t_1 and t_2 provides the spatial information in the f_1 dimension versus the chemical shift information in the f_2 dimension. The profile shown in

figure 14 is deduced from the column (in the two-dimensional map) at the frequency ν_0 corresponding to the water resonance. Would the sample contain other chemical species, Fourier transform of the columns corresponding to their respective resonance frequencies would yield their spatial localization. This is the basis of CSI (Chemical Shift Imaging) by B_1 gradients, much simpler to implement than the conventional methods using B_0 gradients [26]. The latter imply first an rf pulse to take magnetization in the measuring plane and after the evolution period spin echo detection for avoiding the effects of the unavoidable fall time of B_0 gradients. Figure 14 can be considered as a significant result for B_1 gradient CSI methodology, which can be run with a *single* gradient period followed *immediately* by data acquisition.

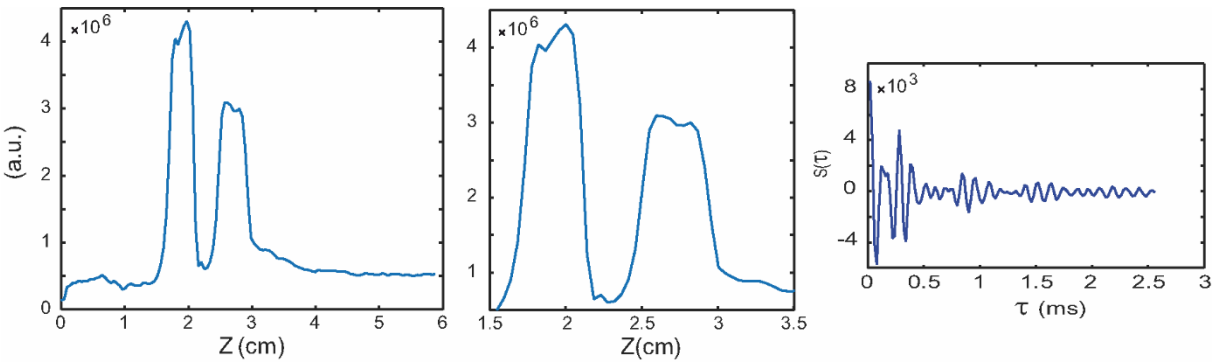

Fig. 14. Left: A spatial profile as obtained by the sequence of figure 13 for a phantom made of a 10 mm o.d. NMR tube containing water sequestered in two compartments of about 0.5 cm length separated by a spacer of the same length. Notice the sharp edges corresponding to the two compartments indicating an exceptional spatial resolution. Center: expansion of the left spectrum. Right: the pseudo-fid obtained at the frequency of water NMR signal and leading to the left spectrum after Fourier transform (see text), $\tau\,(\equiv t_1)$ corresponds to the duration of the B_1 gradient pulses.

CONCLUSION

The aim of this work was the design and construction of a novel coil system capable of producing a high quality B_1 gradient in the direction of the symmetry axis of this coil system and thus able to accommodate usual vertical NMR sample tubes. Although this represents a

relatively modest volume, it can be anticipated that this limitation could be lifted and that a larger volume could be easily reached by a homothetic transformation of the present setup.

This device has first been successfully checked by diffusion measurements and then by a sequence aiming at chemical shift imaging. In each case, one can take advantage of the specific features of a B_1 gradient which involves negligible rise and fall times and which is capable on acting on any component of the nuclear magnetization. These features lead invariably to experimental conditions which are simpler and, maybe, more efficient than their counterparts with B_0 gradients. In particular, it can be anticipated that the B_1 gradient method could be quite suitable for Chemical Shift Imaging (CSI) experiments.

REFERENCES

[1] D. Canet, Radiofrequency field gradient experiments, Prog. Nucl. Magn. Reson. Spectrosc. 30, (1997) 101-135.
[2] A. Haase, C. Mallay, G.K. Radda, Spatial localization of high resolution ^{31}P spectra with a surface coil, J. Magn. Reson. 55 (1983) 164-169.
[3] G.S. Karczmar, D.B. Twieg, T.J. Lawry, G.B. Matson, M.W. Weiner, Detection of motion using B_1 gradients, Magn. Reson. Med. 7 (1988) 111-116.
[4] D. Canet, B. Diter, A. Belmajdoub, J. Brondeau, J.C. Boubel, K. Elbayed, Self-diffusion measurements using radio-frequency field gradients, J. Magn. Reson. 81 (1989) 1-12.
[5] D. Boudot, D. Canet, J. Brondeau, Spatial labeling by a radio-frequency field gradient. DANTE-Z profile, probed by one-dimensional nutation imaging, J. Magn. Reson. 87 (1990)385-394.
[6] D. Bourgeois, M. Decorps, A gradient method for the detection of slow coherent motion, J. Magn. Reson. 91 (1991), 128-135.
[7] R. Kimmich, B. Simon, H. Köstler, Magnetization-grid rotating-frame imaging technique for diffusion and flow measurements, J. Magn. Reson. A112 (1995) 7-12.
[8] F. Humbert, B. Diter, D. Canet, NMR microscopy by strong radio-frequency field gradients with spatial resolution better than five micrometers, J. Magn. Reson. A123 (1996) 242-245.
[9] C. Malveau, B. Diter, P. Tekely, D. Canet, Chemical shift imaging in rotating solids by radio-frequency field gradients, J. Magn. Reson. 134 (1998) 171-175.
[10] J.F. Kuntz, G. Trausch, P. Palmas, P. Mutzenhardt, D. Canet, Diffusive diffraction phenomenon in a porous polymer material observed by NMR using radio-frequency field gradients, J. Chem. Phys. 126 (2007) 134904.
[11] K.C.H. Tijssen, J. Bart, R.M. Tiggleaar, J.W.G. (Hans) Janssen, A.P.M. Kentgens, P.J.M. van Bentum, Spatially resolved spectroscopy using tapered stripline NMR, J. Magn. Reson. 263 (2016) 136-146.
[12] L. Guendouz, S. Leclerc, A. Retournard, A. Hedjiedj, D. Canet, Single-sided radio-frequency gradient with two unsymmetrical loops: application to nuclear magnetic resonance, Rev. Scient. Instrum. 79 (2008) 123704.
[13] J.O. Friedrich, R. Freeman, a "straddle coil" for *in vivo* NMR, J. Magn. Reson. 68 (1986) 582-587.
[14] J. Friedrich, R. Freeman, Spatial localization using a "straddle coil", J. Magn. Reson. 77 (1988) 101-118.
[15] K. Woelk, R.R.E. Gerald, J. Klinger, J.W. Rathke, Imaging diffusion in toroid cavity probes, J. Magn. Reson. A121 (1996) 74-77.
[16] J.P. Boehmer, R.I. Prine, R. W. Briggs, The cone coil, a RF gradient coil for spatial encoding along the B_0 axis in rotating-frame imaging experiments, J. Magn. Reson. 83 (1989) 152-159.
[17] I. Ardelean, A. Scharfenecker, R. Kimmich, Two-pulse nutation echoes generated by gradients of the radiofrequency amplitude and of the main magnetic field, J. Magn. Reson. 144 (2000) 45-52.
[18] I. Ardelean, R. Kimmich, A. Klemm, The nutation spin echo and its use for localized NMR, J. Magn. Reson. 146 (2000) 43-48.
[19] D. Sakellariou, C.A. Meriles, A. Moule, A. Pines, Variable rotation composite pulses for high resolution nuclear magnetic resonance using inhomogeneous magnetic and radiofrequency fields, Chem. Phys. Lett. 363 (2002) 25-33.

[20] G. Farrher, I. Ardelean, R. Kimmich, Probing four orders of magnitude of the diffusion time in porous silica glass with unconventional NMR techniques, J. Magn. Reson.182 (2006)215-220.
[21] D. Topgaard, A. Pines, Self-diffusion measurements with chemical shift resolution in inhomogeneous magnetic fields, J. Magn. Reson. 168 (2004) 31-35.
[22] D. Topgaard, D. Sakellariou, A. Pines, NMR spectroscopy in inhomogeneous B_0 and B_1 fields with non-linear correlation, J. Magn. Reson. 175 (2005) 1-10.
[23] W.R. Smythe, *Static and Dynamic Electricity*, 3rd ed., Cambridge University Press, Cambridge, 1999.
[24] F.E. Terman, *Radio Engineers' Handbook*, New York: McGraw-Hill, 1943.
[25] S. Leclerc, L. Guendouz, A. Retournard, D.Canet, NMR diffusion measurements under chemical exchange involving a large chemical shift difference, Concepts Magn. Reason., 36A (2010) 127-137.
[26] R. Pohmann, M. von Kienlin, A. Haase, Theoretical evaluation and comparison of fast chemical shift imaging domain, J. Magn. Reson. 129 (1997) 145-160.

APPENDIX : Detailed calculations for a three-loop system

In the general case of a circular loop of radius a and at an arbitrary distance from the origin O (which is located on its symmetry axis x), the magnetic field along the Ox axis can be calculated by means of the following expansion [23]

$$B_{1,axial}^{SL} = \frac{\mu_0 I}{2R} \sin\alpha \sum_{n=0}^{\infty} P_{n+1}^{1}(\cos\alpha) \left(\frac{x}{R}\right)^n \quad , |x| < R \tag{A1}$$

where I is the current intensity in the loop and μ_0 the air permeability.

The various quantities in (A1) are defined in Fig. 1 of the main text; $P_{n+1}^{1}(\cos\alpha)$ is the associated Legendre polynomial.

Consider now the system of three coaxial circular loops in the co-current mode (Fig.2 in the main text). The resulting magnetic field can be expressed as

$$B_{1,axial} = \sum_{n=0}^{\infty} b_n x^n \tag{A2}$$

with

$$b_n = \sum_{i=1}^{3} b_{ni} = \frac{\mu_0 I}{2}\left[\sum_{i=1}^{3} \frac{1}{R_i^{n+1}} \sqrt{1 - X_i^2} P_{n+1}^{1}(X_i)\right], \quad n = 0,1,2 \ldots \tag{A3}$$

where $X_i = \cos\alpha_i$ and where loops are numbered so that $-1 < X_3 < X_2 < X_1 < 1$. The polynomial expressions of $b_{ni}/(\mu_0 I)$ are listed up to $n = 6$ in Table A1 below.

Table A1
b_{ni} coefficients relative to the loop i (see Eq. (A3)).

n	$b_{ni}/(\mu_0 I)$
0	$(1 - X_i^2)/(2R_i)$
1	$3\,X_i(1 - X_i^2)/(2\,R_i^2)$
2	$3(-1 + 6\,X_i^2 - 5X_i^4)/(4\,R_i^3)$
3	$5\,X_i(-3 + 10\,X_i^2 - 7X_i^4)/(4\,R_i^4)$
4	$15(1 - 15\,X_i^2 + 35\,X_i^4 - 21\,X_i^6)/(16\,R_i^5)$
5	$21X_i(5 - 35\,X_i^2 + 63\,X_i^4 - 33\,X_i^6)/(16\,R_i^6)$
6	$7(-5 + 140\,X_i^2 - 630\,X_i^4 + 924\,X_i^6 - 429\,X_i^8)/(32\,R_i^7)$

The classical method for producing a uniform gradient consists in the cancellation of derivatives calculated from the B_1 expression, starting from order 2 up to the maximum order

which can lead to a derivative equal to zero. Equivalently, for an axial magnetic field and referring to Eq. (A2), this amounts to solve the following equations

$$b_n = 0 \qquad (n = 2,3, \dots). \tag{A4}$$

For our three-coil system, $b_2 = 0$ leads to the following equation.

$$(-1 + 6\,X_1^2 - 5X_1^4) + R_{12}^3(-1 + 6\,X_2^2 - 5X_2^4) + R_{13}^3(-1 + 6\,X_3^2 - 5X_3^4) = 0 \tag{A5}$$

In order to minimize the number of parameters, we have introduced the following quantities $R_{12} = R_1/R_2$ and $R_{13} = R_1/R_3$.

Eqs. (A6) and (A7) below correspond to the third and fourth orders, respectively.

$$X_1(-3 + 10\,X_1^2 - 7\,X_1^4) + R_{12}^4\,X_2(-3 + 10\,X_2^2 - 7\,X_2^4) + R_{13}^4\,X_3(-3 + 10\,X_3^2 - 7\,X_3^4) = 0, \tag{A6}$$

$$(1 - 15\,X_1^2 + 35\,X_1^4 - 21\,X_1^6) + R_{12}^5(1 - 15\,X_2^2 + 35\,X_2^4 - 21\,X_2^6) + R_{13}^5(1 - 15\,X_3^2 + 35\,X34 - 21\,X36 = 0. \tag{A7}$$

In a first attempt to solve eqs. (A5-A7), we can consider that the three loops are positioned within a sphere so that $R_{12} = R_{13} = 1$. In spite of many solutions in terms of X_1, X_2 and X_3, it turns out that, owing to the restrictions on the X_i $(-1 < X_3 < X_2 < X_1 < 1)$, only two configurations are possible. In fact, for one of these two configurations, terms of order higher than four are much lower than for the other configuration. This configuration denoted TL_S leads, in practice, to a perfectly uniform gradient and corresponds to $X_{1S} = 0.7543569$, $X_{2S} = 0.5007449$, $X_{3S} = -0.04951735$. Using Biot-Savart Law and the data of Table A2 below, the expression of the relevant rf field along the axis common to the three coils is as follows (with rounded coefficients)

$$B_{1,axial}^{TL_S} \approx \left(\frac{\mu_0 I}{a_3}\right)[1.0875 + 0.9739\left(\frac{x}{a_3}\right) - 1.1226(\frac{x}{a_3})^5 - 1.1610(\frac{x}{a_3})^6 + \cdots] \tag{A8}$$

where a_3 is the radius of the largest coil (the third coil). Note that with the considered accuracy for the roots, the zero coefficients of the expansion remain less than 10^{-6}.

Going to a non-spherical configuration (with the unknowns $X_{1,2,3}$, R_{12} et R_{13}), we have to solve the first five equations extracted from Table A1. Preliminary calculations with only four equations (Eq. (A4) for $n = 2, \dots, 5$) indicate numerically that possible solutions exist i) for values of R_{12} and R_{13} close to 1 and 0.8, respectively, ii) angles such that X_1 close to X_{1S}, X_2 and X_3 being slightly greater than X_{2S} and X_{3S}, respectively. Owing to the concavity of the whole system, we can look for a configuration where an ellipsoid replaces the sphere of the above calculations. In that case, it can be shown that, for R_{12} increasing in the interval $[0.9702, 1.0269]$, R_{13} must increase in the interval $[0.7854, 0.8823]$. In these intervals, there exists an optimal configuration for which $b_6 = 0$. This configuration, denoted TL_E, corresponds to: $R_{12} = 0.9889916$, $R_{13} = 0.8290353$, $X_{1E} = 0.7804762$, $X_{2E} = 0.3406291$ and $X_{3E} = -0.1976708$. Proceeding as for Eq. (A8), the relevant expression of the rf field is in this case as follows:

$$B_{1,axial}^{TL_E} = \left(\frac{\mu_0 I}{a_3}\right)\left[1.2189 + 0.9836\left(\frac{x}{a_3}\right) - 3.1954\left(\frac{x}{a_3}\right)^7 - 7.6444\left(\frac{x}{a_3}\right)^8 + \cdots\right]. \qquad \text{(A9)}$$

Table A2
Dimensions (relatively to the radius a_3 of the main loop) of the considered gradient-coils. Origin corresponds to the center of the gradient field.

		Coils		
Loops		*SL*	TL_S	TL_E
outer	radius	1	1	1
	distance from O	0.5	−0.0495782	−0.2016497
middle	radius		0.8666580	0.8039973
	distance from O		0.5013600	0.2912843
inner	radius		0.6572709	0.5287335
	distance from O		0.7552834	0.6600665

Declaration of Competing Interest

None.

Funding: This research did not receive any specific grant from funding agencies in the public, commercial, or not-for-profit sectors.

Graphical abstract